# Impurity modes in one-dimensional periodic systems: The transition from photonic band gaps to microcavities

R. P. Stanley, R. Houdré, U. Oesterle, and M. Ilegems
*Institut de Micro- et Optoélectronique, Ecole Polytechnique Fédérale de Lausanne, CH-1015 Lausanne, Switzerland*

C. Weisbuch
*Thomson-CSF, Laboratoire Central de Recherches, Domaine de Corbeville, F-91404 Orsay CEDEX, France*
(Received 22 March 1993)

We present a unified model of photonic-band-gap impurities and optical microcavities by using a one-dimensional distributed Bragg reflector. A variable-width center layer creates impurity photon states within the photonic band gap. We show that the best optical features (light localization, electric-field strength, linewidth, and laser threshold gain) are obtained when the layer thickness is half-wave (or a multiple), in which case the photon impurity state is located at the middle of the photonic band gap and the structure is a $\lambda/2$ (or higher-order) Fabry-Pérot microcavity.

PACS number(s): 42.50.−p

The optical properties of solids are characterized as broad optical features that occur because there is a continuum of both electron states and photon modes allowing transitions for a wide range of energies and directions. The primary way to obtain sharp optical features is through control of the electronic states in solids by the use of quantum-confined structures [1]. With this aim, electronic band-gap engineering is moving towards the "ultimate" quantized system of zero-dimensional (0D) quantum boxes for which only discrete quantized states exist. In this system the electrons have a single discrete ground-state energy and their oscillator strength is concentrated at atomiclike transitions. Alternatively, sharp optical features may be obtained through photon-mode selection. In 1946, Purcell [2] showed that spontaneous emission in a vacuum occurs into a continuum of photon modes, and that by reducing the number of allowed photon modes the line shape, strength, and direction of spontaneous emission could be controlled. One method, suggested by Yablonovitch [3,4] and John [5,6], is to use three-dimensional periodic structures to create a photonic band gap (PBG). In analogy to solid-state electronics, the wave propagation in a periodic structure gives rise to a PBG. Impurity states within the band gap can localize light and radically alter the emission characteristics of resonant luminescent centers. A second, complementary approach championed by Yamamato [7,8], Yokoyama [9,10] and their colleagues [11] concentrates on microcavity structures, which quantize the photon modes by size effects. When the dimensions of the cavity are similar to the wavelength of light, some resonant modes are enhanced, while most of the other vacuum modes are inhibited. Microcavities have been successful in atomic physics in producing strong photon-atom–coupling phenomena, such as one-atom masers [12], Rabi splitting [13], and quantum nutation [14]. Recent observation of vacuum Rabi splitting in a monolithic microcavity shows that the strong-coupling regime is also achievable in semiconductors [15].

In this paper we intend to compare the two approaches: impurities in photonic band gaps and quantum microcavities. We use a well-known physical system, the multilayer quarter-wave-stack distributed Bragg reflector (DBR). By making one of the layers in the structure of variable width, we can move continuously from a perfect PBG material to one with an impurity that localizes light, to a microcavity, and then back to a PBG in a cyclical fashion. This analogy between DBR's and PBG systems has already been mentioned by Yablonovitch [3]. We present here a systematic quantitative analysis of such a system. By calculating numerically the local-field intensity and the threshold gain for all cases, we directly compare the potential efficiency of photon-mode control of these classes of structures. From this analysis it will become clear that the Fabry-Pérot (FP) microcavity is not only a special case of an impurity mode, the midgap one, but it is also the best impurity mode for producing the maximum local-field intensity, the strongest localization of light, and the lowest gain threshold.

The modeled structure is based on classic Bragg mirror structures using alternating $\lambda/4$ layers of GaAs and AlAs, consisting of (20 pairs of GaAs-AlAs–a GaAs "impurity" layer)–(20 pairs of AlAs-GaAs) (Fig. 1). The front and back surfaces are air. The refractive indices of GaAs and AlAs are 3.56 and 2.95, respectively. We choose the dimensions of the layers such that $hc/\lambda = 1$ eV, except for the middle layer, which is varied. We use the standard method of matrices to calculate the transmission of the stack as well as the field intensity throughout the structure [16]. The matrices are based on a scalar plane-wave solution to Maxwell's equations. It should be noted that although the vector nature of light leads to erroneous results for the scalar plane wave in predicting three-dimensional photonic band gaps [17–19], the solutions are completely separable in the one-dimensional case and degenerate at normal incidence.

The transmission of the structure with a $\lambda/4$ "impuri-

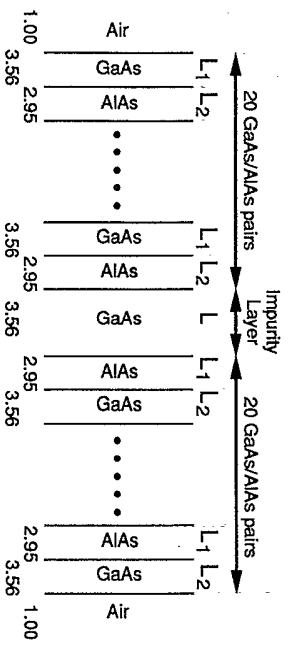


FIG. 1. Schematic of Bragg stack used in this paper. The middle layer has a variable width and acts as an impurity. The refractive index of each layer is shown.

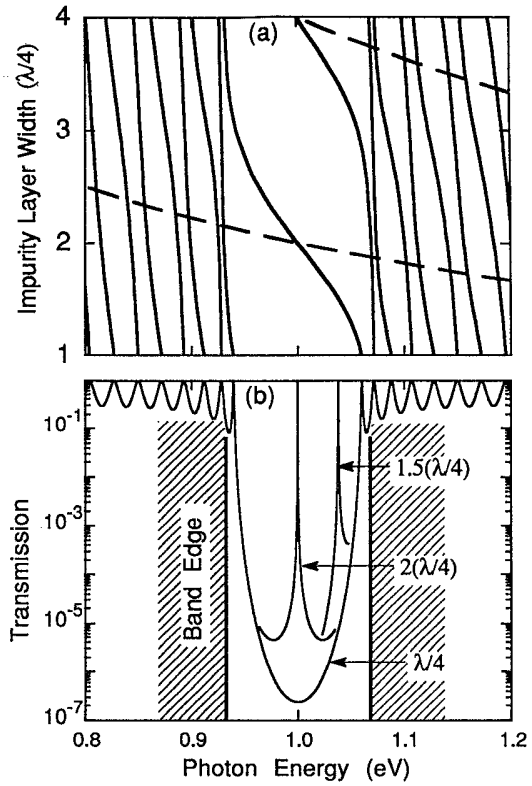


FIG. 2. (a) The position of transmission maxima as a function of "impurity"-layer width for a DBR structure (solid lines) and a FP étalon of the same dimensions as the "impurity" layer (dashed lines). (b) Transmission of a $\lambda/4$ DBR stack as a function of photon energy. The transmission peak on the high-energy side of the stop band moves into the stop band as shown for $1.5(\lambda/4)$ and $2(\lambda/4)$ "impurity"-layer widths. The horizontal scale (photon energy) is the same for both (a) and (b). Hatched areas denote the allowed bands.

ty" layer, for which the complete structure acts as a Bragg mirror, is shown in Fig. 2(a) (curve labeled $\lambda/4$). The transmission has a broad minimum or stop band from 0.93 to 1.07 eV. On either side of the stop band, there is a series of sidelobes, with maxima reaching unity transmission. At these energies light can propagate unimpeded through the structure. We call the two transmission peaks nearest the stop band band-edge modes. These represent the lowest- (highest-) energy photons that can propagate freely outside the stop band.

For a $\lambda/2$ "impurity" layer we satisfy the FP condition and a transmission maximum occurs in the center of the stop band [Fig. 2(b), curve labeled $2(\lambda/4)$]. This structure is a $\lambda/2$ cavity between two DBR mirrors. For intermediate "impurity"-layer widths, the structure is neither a perfect DBR nor a perfect Fabry-Pérot microcavity. Instead, the first high-energy transmission peak (edge mode) of the perfect mirror moves into the stop band and becomes a "FP-like" maximum [20]. The position of the transmission maxima as a function of layer width and energy is shown in Fig. 2(b). This plot shows that with increasing layer width the high-energy band-edge transmission peak splits away from the others and moves into the stop band. The peak moves across the stop band and merges with the band of transmission maxima at low energies. This pattern repeats itself as a function of layer width every $\lambda/2$. The dashed lines in Fig. 2(a) show the position of the FP maxima for a Fabry-Pérot étalon with the same width as the impurity layer. For impurity-layer widths of $N(\lambda/2)$, the positions of the transmission maxima are the same for both a FP étalon and the DBR structure. The reason for this structure behaving unlike a FP étalon for intermediate widths is that, in a FP étalon a standing wave is set up between only two reflecting surfaces, while in a DBR structure there are $2N$ interfaces on each side for $N$ mirror pairs. It is only for a $\lambda/2$ layer that a standing wave between the first two interfaces will simultaneously satisfy the boundary conditions for all interfaces.

The similarity between this picture and that of electrons propagating in a one-dimensional solid is striking [21–23]. (Compare our Fig. 2(a) and Fig. A2-6 of Ref. [23].) For a solid with $N$ unit cells, there are bands of $N$ eigenstates. These correspond to Bloch waves that can propagate through the crystal. If a localized defect is introduced, the energy eigenstates are perturbed, producing a small shift of all the band states except for one of the states at the band edge, which moves into the forbidden region and becomes an impurity state. Whether this state splits off the top or bottom band edge depends on the sign of the impurity potential. Once in the forbidden region, the electron has an evanescent envelope function and becomes localized at the impurity site. Within the band there are symmetric and antisymmetric electron states, and these show a crossing behavior with increasing perturbation energy. In the Bragg mirror, there are also $N$ transmission maxima, which correspond to optical Bloch waves that can travel through the mirror. The introduc-

tion of a wider layer causes a defect in the structure. One of the band-edge transmission peaks moves into the stop band to become an impurity mode, while other transmission maxima outside of the stop band move slightly in energy and display an anticrossing behavior.

From the analogy with solid-state electronics we use the terms band-edge modes, unbound modes, and impurity modes to denote the transmission maxima at the stop band, outside the stop band, and inside the stop band, respectively. In this terminology the perfect FP structure corresponds to a deep-center midgap impurity state. The exact behavior of these photonic band-gap states [Fig. 2(b)] is identical to the band structure of impurities shown in classic texts on solids [21–23], except for the anticrossing behavior. The impurity used to model electronic states is usually represented by a $\delta$ function in space. Antisymmetric states are unperturbed in such a model as they have a node at the impurity site. The finite spatial extent of the impurity in our model results in mixed symmetric and antisymmetric photon modes, which results in anticrossing behavior.

Clearly, the allowed photon modes in a one-dimensional band-gap structure are very different from the vacuum, and this alters the spontaneous emission properties of fluorescent centers embedded in such a structure. The degree to which the spontaneous emission is altered depends on the distribution and the strength of the photon modes. In particular, we are interested in the field intensity at the luminescent and/or gain region of our structure, which, in practice, can be one or more quantum wells placed in or near the "impurity" layer. To evaluate different impurity modes, it is important to know the maximum field intensity inside the structure and how the field is distributed spatially.

Figure 3(a) shows the envelope of the field intensity across the length of the test structure for various conditions. The field intensity oscillates in a standing-wave pattern across the length of the structure [inset of Fig. 3(a)] and the envelope of the field intensity changes for various conditions. A $\lambda/4$ "impurity"-layer width generates a DBR with edge modes. The envelope field intensity for the high-energy edge mode is just visible in Fig. 3(a). Increasing the layer width to $\lambda/2$ produces a perfect FP structure for which the maximum field intensity is two orders of magnitude larger than for a band-edge mode. The strong peak of the field at the "impurity" layer and the exponential decay of the field away from the impurity illustrates the localization of light at an impurity center.

As the width of the "impurity" layer is changed, the impurity mode changes energy and the maximum field intensity also changes. By varying the "impurity"-layer thickness, we can examine the variation of maximum field intensity of the impurity mode as it traverses the PBG. This is shown in Fig. 3(b), where hatched areas denote the allowed bands. The largest field occurs when the impurity mode is exactly at the midgap energy, and it decays rapidly when it shifts towards the band edges where the localization of light is also weak. It should be noted that for the unbound modes there is little enhancement of the field intensity, so that these do not show up

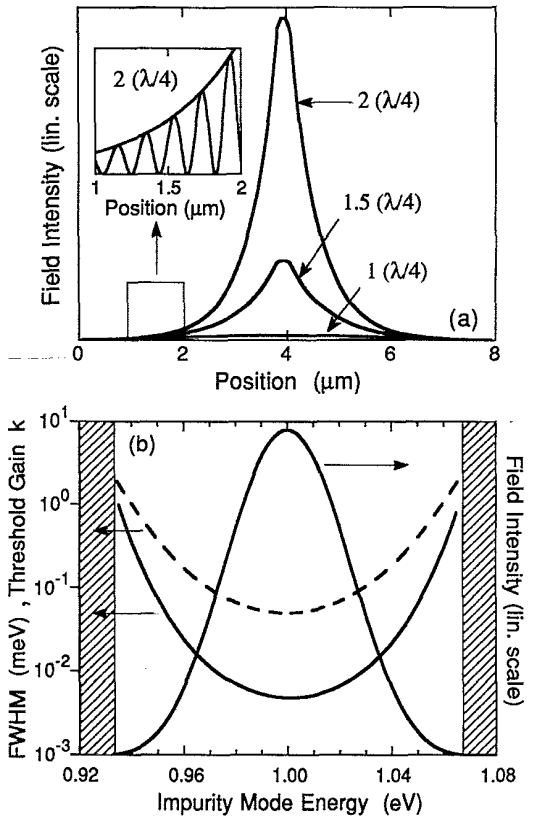


FIG. 3. (a) The envelope field intensity inside the DBR stack for different "impurity"-layer widths. Inset shows the oscillating electric field for the $2(\lambda/4)$ case. (b) The variation of the maximum field intensity as a function of impurity-mode energy (right-hand axis). Dashed line shows the spectral width (full width at half maximum) in meV (left-hand axis). Also shown is the dimensionless gain threshold $k$ as a function of impurity-mode energy (left-hand axis).

on the plot. The enhancement of the impurity modes as deep centers in the midgap or FP region can be seen. In addition to the decrease in the spatial extent of the field intensity of the impurity mode, there is also a decrease in its spectral width. These two effects combine to give the large resonant enhancement of the electric field at the impurity mode. The variation in linewidth is shown as a dashed line in Fig. 3(b). The decrease of the spectral width follows the increase of the effective FP finesse. This decrease in spectral width is an important property for future device prospects and, again, the midgap impurity mode shows the best features with the narrowest spectral width or highest finesse.

The ultimate criterion for evaluating PBG structures and microcavities as laser resonators is not maximum local-field intensity but rather threshold gain, $g_{th}$. In order to calculate $g_{th}$ we first have to select the most favorable position for the gain medium. By examining the field intensity inside the structure, the position of maximum field intensity is known. From symmetry, this is found to be either in the middle of the "impurity" layer or at the first antinode to either side. Thus, to simulate a

gain medium we use two layers similar in thickness to a quantum well (50 Å) and place them at the positions of maximum field intensity. For simplicity, the gain medium is made dispersionless and the wavelength of the lasing mode is determined by the length of the "impurity" layer. The threshold gain can be calculated using the matrix method by noting the quantum-well gain at which the transmission of the structure diverges to infinity.

The variation of $g_{th}$ as a function of "impurity"-layer width is shown in Fig. 4. We have used the imaginary part of the refractive index, $k$, as a dimensionless gain parameter. (Using $g=4\pi k/\lambda_0$, where $\lambda_0$ is the lasing wavelength, $k=0.1$ corresponds to $g_{th}=10^4$ cm$^{-1}$, the saturated gain value for a quantum well, while $k=0.01$ is a more realistic gain level.) The threshold gain $g_{th}$ decreases as the "impurity"-layer width increases from a $\lambda/4$ DBR to a $\lambda/2$ FP structure. A further increase in layer width leads to an increase in $g_{th}$ until at $3(\lambda/4)$ the structure behaves like a DBR again. The change in layer width causes a continuous change in lasing energy. For layers just thicker than $3(\lambda/4)$ the lasing position jumps to higher energies and $g_{th}$ starts to drop once more. The pattern repeats itself every $\lambda/2$, except that the regions of minimum $g_{th}$ become broader. This is connected to the nonuniform change in energy with layer width. As with the field intensity, the value of $g_{th}$ is the same for a given lasing energy regardless of layer width. The variation of $g_{th}$ with energy is shown in Fig. 3(b). There is a drop in $g_{th}$ by two orders of magnitude between edge modes, the impurity mode, and midgap FP modes. This improvement is due to both the spatial localization of field intensity and its reduced spectral width. Figures 3(b) and 4 show that structures operating on edge modes make unrealistic laser resonators, although strong nonlinearities have been associated with such modes [24]. Only deep impurities, i.e., cavities close to $N(\lambda/2)$ in length, make efficient laser structures. The threshold gain is found to be the same for both $\lambda/2$ and $\lambda$ "impurity"-layer (cavity) widths. However, in this model there are no losses due to absorption or diffraction, as a one-dimensional plane wave is used. In a real structure losses favor the use of smaller structures so that the light spends more time in the gain region rather than in loss regions.

The extension of these calculations to three dimensions is not trivial, and although the treatment here is for a one-dimensional PBG material, 3D considerations would lead to similar results. Some interesting questions do arise by extending the qualitative results to 3 dimensions. While it has been shown here that the midgap FP impurity shows the strongest localization of light, the maximum field intensity, and the lowest lasing threshold, what is the three-dimensional equivalent of a perfect FP structure? It is quite simple to generate an impurity which "sits" at midgap energy in one part of the Brillouin zone, but this may be far from midgap at other symmetry positions, as would be the case for suggested band-gap structures. On the other hand, this may be advantageous for a directional emitter. PBG structures with very wide band gaps would make this variation unimportant. Alternatively, using the microcavity approach, a distributed Bragg "onion," starting with a $\lambda/2$ sphere encapsulated by alternating $(\lambda/4)$ thick shells, would have a perfect FP mode in all directions.

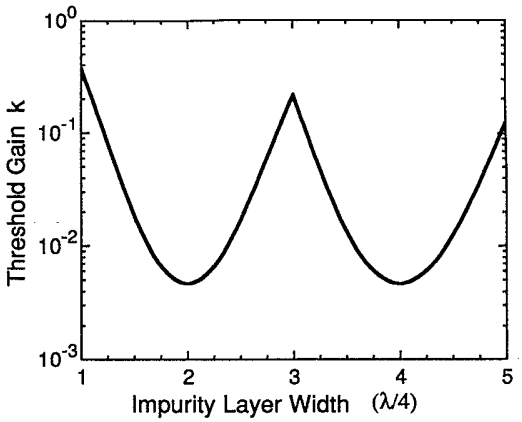


FIG. 4. The variation of dimensionless gain threshold $k$ as a function of "impurity"-layer width. The discontinuity at $3(\lambda/4)$ is due to a change in the lasing wavelength with minimum gain from one band edge to the other.

In conclusion, in this paper we have brought together the PBG and microcavity approaches to photon-mode control. In one dimension, edge modes, impurity modes, and FP microcavities are general features of PBG's. The perfect FP microcavity is identical to a midgap impurity mode, and this mode is the best for localizing light, for maximizing the field intensity, and for producing the lowest-gain threshold in a laser resonator. While we have shown that the best impurity mode in a PBG is the $\lambda/2$ midgap impurity, it will be a matter of fabrication difficulty to decide which implementation to choose: either a 3D standard PBG material or any other physical realization of a 3D microcavity.

This work was supported under a joint Thomson-CSF (France) and Ecole Polytechnique Federale de Lausanne (EPFL) (Switzerland) program.

[1] C. Weisbuch and B. Vinter, *Quantum Semiconductor Structures: Fundamentals and Applications* (Academic, Boston, 1991).
[2] E. M. Purcell, Phys. Rev. **69**, 681 (1946).
[3] E. Yablonovitch, Phys. Rev. Lett. **58**, 2059 (1987); E. Yablonovitch and T. J. Gmitter, Phys. Rev. Lett. **63**, 1950 (1989).
[4] E. Yablonovitch, T. J. Gmitter, and K. M. Leung, Phys. Rev. Lett. **67**, 2295 (1991).
[5] S. John, Phys. Rev. Lett. **58**, 2486 (1987).
[6] S. John and R. Rangarajan, Phys. Rev. B **38**, 10 101 (1988).
[7] Y. Yamamoto, S. Machida, and G. Björk, Phys. Rev. A **44**, 657 (1991).
[8] Y. Yamamoto, S. Machida, K. Igeta, and G. Björk, in *Controlled Spontaneous Emission in Microcavity Semiconductor Lasers*, edited by Y. Yamamoto (Wiley, New York,

1991), p. 561.
[9] H. Yokoyama, K. Nishi, T. Anan, H. Yamada, S. D. Brorson, and E. P. Ippen, Appl. Phys. Lett. **57**, 2814 (1990).
[10] H. Yokoyama, M. Suzuki, and Y. Nambu, Appl. Phys. Lett. **58**, 2598 (1991).
[11] G. Björk, S. Machida, Y. Yamamoto, and K. Igeta, Phys. Rev. A **44**, 669 (1991).
[12] D. Meschede, H. Walther, and G. Müller, Phys. Rev. Lett. **54**, 551 (1985).
[13] R. J. Thompson, G. Rempe, and H. J. Kimble, Phys. Rev. Lett. **68**, 1132 (1992).
[14] G. Rempe, H. Walther, and N. Klein, Phys. Rev. Lett. **58**, 353 (1987).
[15] C. Weisbuch, M. Nishioka, A. Ishikawa, and Y. Arakawa, Phys. Rev. Lett. **69**, 3314 (1992).
[16] A. Yariv and P. Yeh, *Optical Waves in Crystals* (Wiley, New York, 1984), p. 155.
[17] Z. Zhang and S. Satpathy, Phys. Rev. Lett. **65**, 2650 (1990).
[18] K. M. Leung and Y. F. Liu, Phys. Rev. Lett. **65**, 2646 (1990).
[19] K. M. Ho, C. T. Chan, and C. M. Soukoulis, Phys. Rev. Lett. **65**, 3152 (1990).
[20] It is not a true FP transmission maximum because it does not satisfy the usual Airy condition, except at $L=N(\lambda/2)$.
[21] G. H. Wannier, *Elements of Solid State Theory* (Greenwood, New York, 1970), p. 178.
[22] A. Davydov, *Théorie du Solide* (Mir, Moscow, 1976), p. 158.
[23] J. C. Slater, *Insulators, Semiconductors, and Metals* (McGraw-Hill, New York, 1967), p. 292.
[24] J. He and M. Cada, IEEE J. Quantum Electron. **QE-27**, 1182 (1991).